FEL Simulations for the LCLS*

Heinz-Dieter Nuhn

Stanford Linear Accelerator Center, Stanford University, Stanford, CA 94309-0210, USA

Abstract

A first Design Study Report has recently been completed [1] for the Linac Coherent Light Source (LCLS), a proposal to build an x-ray Free Electron Laser (FEL) at the Stanford Linear Accelerator Center (SLAC) as a single pass SASE (Self-Amplified Spontaneous Emission) amplifier. The proposal includes the use of a very low emittance electron beam accelerated up to 15 GeV by the last third of the SLAC linac to produce sub-picosecond x-ray pulses with high brightness and full transverse coherence in a 112-meter long undulator. Many aspects of the FEL design have been analyzed with FEL simulation codes. The paper discusses some of the results of these aspects, i.e. temporal x-ray pulse structure and power sprectrum, trajectory errors and effects of undulator beam tube wakefields.

1 INTRODUCTION

SLAC and collaborating institutions are proposing to build the LCLS, an FEL facility operating in the wavelength range 1.5-15 Å. Since optical cavities are not available for the wavelength range of interest, due to the lack of good reflecting surfaces to form the optical cavity mirrors, the LCLS is based on the process of SASE [2]. No mirrors are used. Lasing is achieved in a single pass of an electron bunch through a long undulator. The basic parameter set for the proposed LCLS FEL is displayed in table 1 for the short wavelength limit. The design of the LCLS is based on a hybrid permanent magnet undulator that comprises 52 segments each 1.92 m long separated by 24 cm long gaps. The total length of the segments is 99.84 m or 3328 undulator periods. Between the segments are electron beam position monitors and permanent magnet quadrupole magnets for focusing and trajectory control. The discussion in this paper is focused on the short wavelength limit of the LCLS proposed operational range.

2 TIME DEPENDENT SIMULATION RESULTS FROM GINGER

The analysis of startup from noise, saturation, as well as the temporal and spectral structure of the radiation pulse for the LCLS design uses the 2D, time-dependent simulation code

Table 1: Basic LCLS FEL Parameters.

Radiation Wavelength λ_r	1.5 Å
Undulator Period λ_u	3 cm
Peak Magnetic Field	1.32 T
a_w	2.62
Electron Energy	14.35 GeV
Norm. Electron Beam Emittance	1.5 mm mrad
Peak Current	3400 A
RMS Bunch Length	20 μm
Uncorrelated Energy Spread	2.0×10^{-4}
FEL Parameter (1D)	4.7×10^{-4}
Rayleigh Length	40 m
Power Gain Length L_G	5.8 m
Error Free Saturation Length	94 m

GINGER [3, 4], which models the interaction of the 3D motion of the electron beam with an axisymmetric, multi-frequency radiation field. SASE startup from shot noise is modeled by adding random fluctuations to the macro-particles' longitudinal and transverse coordinates [5]. Segment separations or lumped
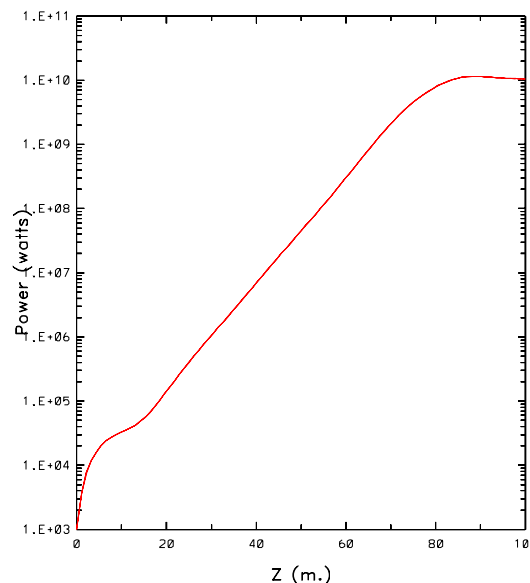

Figure 1: Predicted development of the peak radiation power. The Power is averaged over a window.

focusing are not implemented in GINGER. It has been shown that for the LCLS, and particularly at the short wavelength limit, they have little effect on output power and on the amount of magnet material needed [1]. Output power increase will, of course, pause between segments. Figures that depend on the longitudinal coordinate, z, would show the effect.

Figure 1 shows the development of the pulse averaged peak

power for the error-free LCLS undulator. Exponential growth starts after roughly 15 m. Saturation occurs before the end of the undulator.

In order to reduce the simulation time for the analysis, GINGER is run in a mode in which both the longitudinal electron beam distribution and the radiation field are assumed to be periodic, with a period much larger than the total slippage length. The simulation is only done for one periodicity window. Electron beam slices that slip outside the window on one side will enter it again on the other side. The use of periodic boundary conditions is not believed to lead to significant, unphysical effects. Periodic boundary conditions can not be used to study the effect of correlated energy spread and bunch emittance or electron bunch end effects.

Figure 3: Predictition of the development of the temporal structure of a typical LCLS x-ray pulse along the Undulator. A short periodicity window is used for clarity.

locity v_s is thus predicted to $v_s = c(1 - 2/3 \times \lambda_r/\lambda_u)$ or $1 - v_s/c = 2/3 \times \lambda_r/\lambda_u = 0.33 \times 10^{-10}$, i.e., in the exponential gain regime spikes fall behind the radiation field by $1/3 \times \lambda_r$ every undulator period or they move ahead of the electron beam by $2/3 \times \lambda_r$ during the same time. The simulation predicts a value of $1 - v_s/c \approx 0.3 \times 10^{-10}$, slightly smaller than the prediction of the 1D theory.
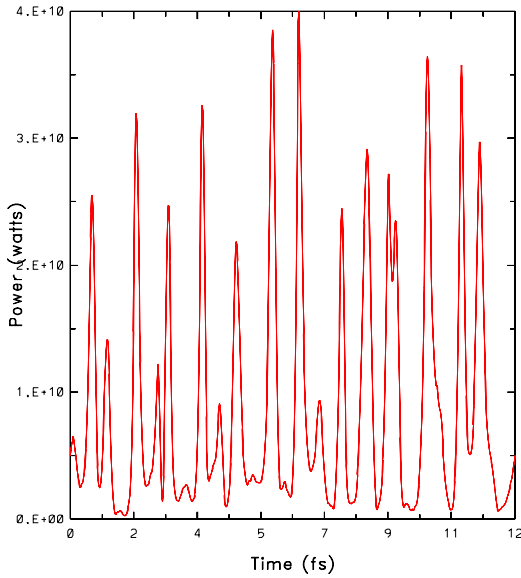

Figure 2: Predicted temporal structure of a typical LCLS x-ray pulse after saturation.

Figure 2 shows the time structure of the radiation field for a periodicity window of 12 fs at the end of a 100 m long undulator. The optical pulse is composed of a number of superadiant spikes spaced at a distance related to the cooperation length $2\pi L_c = 4\pi L_G \lambda_r/\lambda_u = 1.2$ fs $\times c$ as predicted from 1D theory [6].

Figure 3 shows the normalized intensity of the radiation pulse along the window (abscissa) as function of the windows position within the undulator (ordinate). After the initial random distribution in the lethargy regime, and until saturation, a superadient spike structure forms with a group velocity different from the phase velocity of the radiation. The window position is coupled to the phase of the radiation. The group velocity of the spikes was derived in [6] to be $v_s = 3v_\parallel/2 + v_\parallel/c$. Using $v_\parallel = c(1 - \lambda_r/\lambda_u)$ for the average longitudinal speed of the electron beam and the fact that $\lambda_u \ll \lambda_r$, the spike ve-
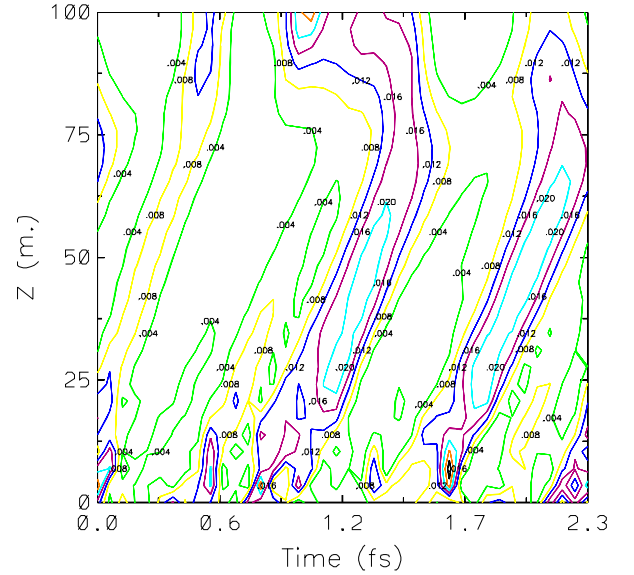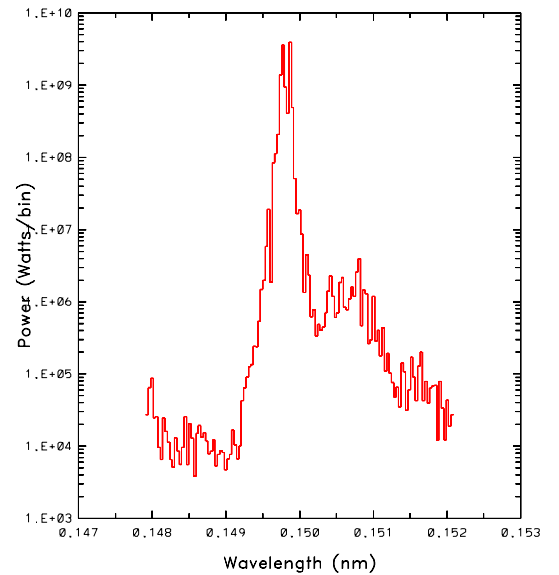

Figure 4: LCLS Spectrum of a longitudinal pulse slice of a typical x-ray pulse around Saturation

The analysis of beam transport from the gun to the undulator through linac and bunch compressors predicts that a correlation between the average energy and the transverse position

of a slice of the bunch and its longitudinal position within the bunch is to be expected. At the entrance to the undulator, the electron bunch is expected to be homogeneous in intensity over most of its core longitudinal position (s. [1] p.7-10). Over the same range, the average value of the energy distribution follows a slowly varying function (covering an rms width of .1 %) while the width of the distribution stays roughly constant ($\Delta\gamma_{corr} <$ .02 %). At both ends of the bunch is a strong increase in energy spread, which will suppress the production of micro-bunching and radiation enhancement. The energy correlation will widen the spectral distribution of the total radiation pulse to about $2\Delta\gamma_{corr} \approx .02\%$)
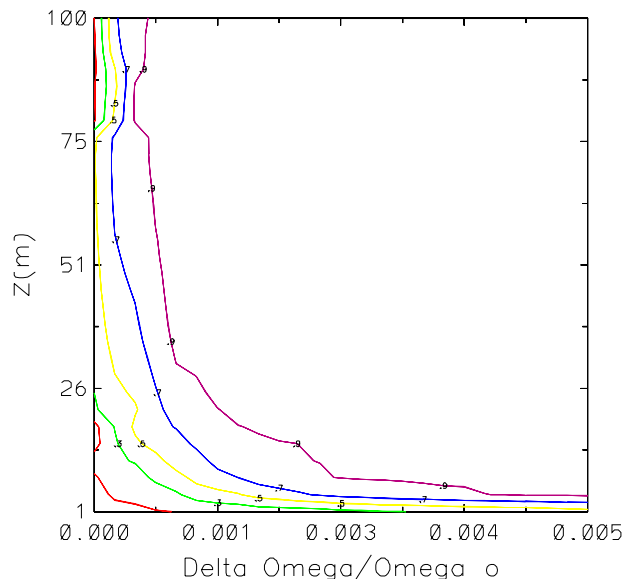

Figure 5: Width of the Power Spectrum of a Longitudinal Slice of the Radiation Pulse vs. Z

Figure 4 shows the predicted spectrum after saturation for a slice from the center region of the radiation pulse. The power is binned into wavelengths intervals of 0.0003 Å. Besides the main spectral line, two other peaks at slightly longer wavelength and lower power level are visible.

Figure 5 shows how the bandwidth of the radiation decreases until saturation is reached. At saturation the rms bandwidth is about $1/N_{sat} \approx 0.003$ as predicted in [7].

3 TRAJECTORY ANALYSIS

Deviations of the electron trajectory from the ideal straight line inside the undulator can be caused by on-axis magnetic field errors, quadrupole misalignments and the limited precision of beam position detection and correction. Trajectory errors can become a major source of gain reduction if they are not kept small. The quadrupoles along the LCLS undulator are made from permanent magnet material and are transversely movable to correct the trajectory in both the horizontal and ver-

tical planes. Thus, the calibration and resolution of the beam position monitor system, not the quadrupole alignment, is the primary source for orbit errors. The choice of high-resolution cavity BPMs and the development of a beam-based-alignment procedure [8] for BPM calibration allow to produce trajectories close to the ideal case. What remains is the random walk trajectory between two beam position monitors caused by magnetic field errors from imperfections of the 128 undulator poles that lie between two LCLS BPM/corrector pairs and from external fields. Shimming in combination with sophisticated field error measurement methods, such as the stretched wire technique, can be used to reduce the random walk trajectory to a very high degree. Extensive FEL simulations have been used to determine the degree of field and trajectory errors that can be allowed before an increase in saturation length occurs.
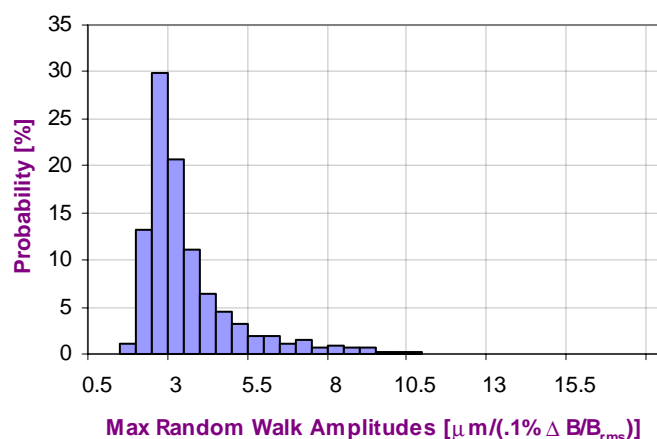

Figure 6: Distributions of the maximum random walk amplitude per rms magnetic field errors for a perfectly steered LCLS orbit. Parameters are $\gamma = 28077$, $\langle\beta\rangle = 18$ m/rad, $\Delta z_{corr} = 2.16$ m

A quantity that is of interest for undulator designers is the rms deviation of the on-axis magnetic field from the ideal case. This quantity can be used as input to the monochromatic 3D simulation code, FRED3D [9]. The specific LCLS undulator field will cause one particular random-walk trajectory, which can only be known after the undulator is built. The simulations use randomly generated Gaussian error distributions with specified rms values, truncated to 3 sigma.

Figure 6 shows the distribution of maximum random walk amplitudes that can be generated by a given rms magnetic field error, assuming that correction occurs every 2.16 m. The distribution peaks below 3 μm/.1% rms error amplitude. Simulations show that up to rms errors of .1 % trajectories at or below the peak of the distribution, i.e. maximum trajectory deviations below 3 μm, will not increase saturation length.

4 WALL ROUGHNESS AND RESISTIVE WALL IMPEDANCE

When the electron beam moves through the undulator it will excite longitudinal and transverse wakefields due to the resistance and the discontinuities of the beam tube wall. The forces due to the wakefields are correlated with longitudinal position, z_1, within the bunch. For a longitudinal bunch slice of length dz, the longitudinal wakefield will generate a change in energy, dγ, at a rate dγ/dz. If the average beam tube properties do not depend on the position within the undulator, a slice's average energy will linearly increase or decrease as it moves along the undulator, depending on its position within the bunch. The transverse electron distribution within a slice is not affected.

If the rate at which the slices' energy change occurs becomes too large, FEL dynamics will be negatively effected due to detrapping. Only the average energy change from this effect can be corrected by tapering. To ensure FEL gain, tolerances for wall roughness and wall resistance need to be established.

In order to simulate the effect with the GINGER code, a position dependent energy loss term $d\gamma_{wake}/dz(z_1) = a\sin(2\pi z_1/b)$ was added to the FEL equations by the author of GINGER [10]. The parameter b specifies the periodicity window width, z_1 is the relative position of a slice within the window, and the amplitude parameter, a, is varied during the study.
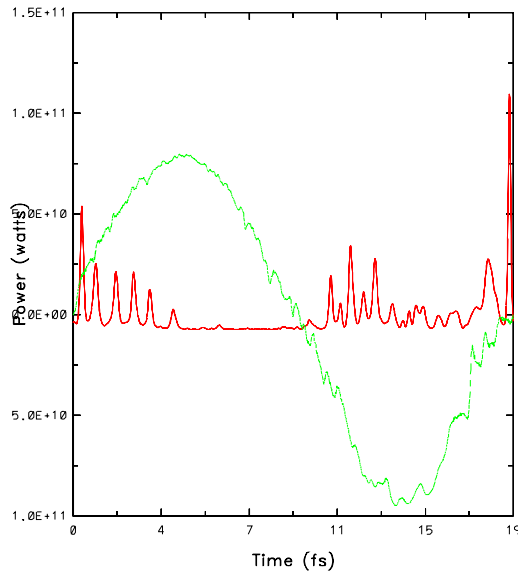

Figure 7: Effect of beam tube wakefields on the temporal structure of the LCLS optical beam. The sinusoidal function corresponds to energy loss of the electron beam the other function to energy gain of the radiation field.

Figure 7 shows the result of a typical run with the parameter values $a = 0.5$ m^{-1} and $b = 18.56$ fs. The ordinate shows the slices' peak power change in units of watts over the length of the undulator, while the abscissa indicates the temporal position of the electron and photon beam slices relative to the beginning of the window at the entrance to the undulator. Note that the electron slices fall behind (i.e. move to the right hand side in the graph) by 1.668 fs with respect to the photon slices during propagation through the undulator, due to slippage. The gain of the radiation spikes is reduced when the energy loss, $\Delta\gamma$, grows outside of the range $-30 \leq \Delta\gamma \leq 20$. For the example shown in the figure, the final reduction in peak power is about one order of magnitude at bunch locations at which the energy loss $\Delta\gamma$ is above this range. The reduction is less at bunch locations where slices gain energy, due to compensation of the electrons' energy loss from radiation. A significant increase in output power occurs at the position where the combination of energy increase from wakefields and the slippage work together to keep the slice in resonance with the ponderomotive potential. For those spikes, growth continues. Saturation does not occur.

The tolerance for the total rms energy change relative to the average bunch energy for a given bunch has been set to 0.001 for the LCLS, which corresponds to a $\Delta\gamma$ of 28. At the present design only a part of the bunch is expected to satisfy this tight tolerance even with wall roughness tolerances as low as 100 nm.

5 REFERENCES

[1] The LCLS Design Study Group, "LCLS - Design Study Report," April 1998. SLAC-R-521.

[2] R. Bonifacio, C. Pellegrini, and L. Narducci, "Collective instabilities and high gain regime in a free electron laser," *Opt. Commun.*, vol. 50, no. 6, 1985.

[3] R.A. Jong, W.M. Fawley, and E.T. Scharlemann, "Modeling of induction-linac based free-electron laser amplifiers," *SPIE*, vol. 1045, pp. 18–27, 1989.

[4] P. Pierini and W.M. Fawley, "Shot noise startup of the 6 nm SASE FEL at the TESLA test facility," in *Proceedings of the Seventeenth FEL Conference (FEL95), New York, NY, USA*, pp. 332–335, August 21 - 25, 1995.

[5] W.M. Fawley, A.M. Sessler, and E.T. Scharlemann, "Coherence and Linewidth Studies of a 4-nm High Power FEL." Proceedings of the 1993 Particle Accelerator Conference, Washington D.C., 1993.

[6] R. Bonifacio et. al., "Spectrum, Temporal Structure, and Fluctuations in a High-Gain Free-Electron Laser Starting from Noise," *Phys. Rev. Let.*, vol. 73(1), p. 70, 1994.

[7] K.-J. Kim, "Three-Dimensional Analysis of Coherent Amplification and Self-Amplified Spontaneous Emission in Free-Electron Lasers," *Phys. Rev. Letters*, vol. 57, no. 15, p. 1871, 1986.

[8] P. Emma, R. Carr, and H.-D. Nuhn, "Beam Based Alignment for the LCLS FEL Undulator." these proceedings.

[9] E.T. Scharlemann, "Wiggle plane focusing in linear wigglers," *J. Appl. Phys.*, vol. 58(6), pp. 2154–2161, 1985.

[10] W.M. Fawley, 1997. Private Communication.